Vapor-Liquid equilibrium measurements for 5 binary mixtures involving HFO-1336mzz(E) at temperatures from 313 to 353 K and pressures up to 2.735 MPa

Eric Boonaert, Alain Valtz, Julien Brocus, Christophe Coquelet, Yannick Beucher, Florence de Carlan, Jean-Marie Fourmigué

Vapor-Liquid equilibrium measurements for 5 binary mixtures involving HFO-1336mzz(E) at temperatures from 313 to 353 K and pressures up to 2.735 MPa.

Eric Boonaert[a], Alain Valtz[a], Julien Brocus[a,b], Christophe Coquelet[a*], Yannick Beucher[b], Florence de Carlan[b], Jean-marie Fourmigué[b]

[a] Mines Paristech, PSL, CTP –Centre of Thermodynamics of Processes, 35 rue Saint-Honoré, 77300 Fontainebleau, France.

[b] EDF LAB LES RENARDIERES – Centre R&D, Moret Loing et Orvanne, 77250, France.

*Corresponding author. E-mail address : christophe.coquelet@mines-paristech.fr. Telephone: +33164694962.

Abstract

Performances of systems using refrigerants are highly dependent on the selection of the working fluids. In order to guide this choice, the thermophysical properties of these fluids need to be correctly correlated. Experimental data are required for models to work; The knowledge of thermophysical properties of working fluids is required for designing ORC and High Pump (HP) systems. Isothermal vapor-liquid equilibrium (VLE) data for the HFO-1336mzz(E) (trans-1,1,1,4,4,4-hexafluoro-2-butene) binary mixture with HFC-290 (Propane), HFC-134a (1,1,1,2-tetrafluoroethane), HFC-152a (1,1-difluoroethane), HFC-227ea (1,1,1,2,3,3,3-heptafluoropropane) and HFO-1234ze(E) (trans-1,3,3,3-tetrafluoropropene) were measured at 313 K, 333 K and 353 K. The experimental technique used is based on static analytic methods. All of the data (*P-x-y*) were well correlated with the Peng-Robinson equation of state, associated with a Mathias-Copeman alpha function and classical mixing rules. The results of such modeling are in good agreement with the measured data.

Keywords: working fluids, phase diagrams, isothermal VLE data, modeling, heat pump, ORC.

Nomenclature

a	Energy parameter of the equation of state ($J.m^3.mol^{-2}$)	b	Molar co-volume parameter of the equation of state ($m^3.mol^{-1}$)
d	Absolute difference	F	Objective function
$k_{i,j}$	Binary interaction parameter	$m_{1,2,3}$	Parameters of the alpha function
N	Number of points	P	Pressure (Pa)
R	Molar gas constant (8.314472 $J.mol^{-1}.K^{-1}$)	T	Temperature (K)
U	Expanded uncertainty	u	Combined uncertainty

v	Molar volume ($m^3.mol^{-1}$)	x	Liquid fraction
y	Vapor fraction		

Greek letters

α	Temperature dependent term	α_{12}	Relative volatility
Δ	Absolute difference	ω	Acentric factor

Subscripts

i,j	Molecular species	c	Critical property
cal	calibration	calc	Calculated
exp	Experimental	rep	repetability

Abbreviations

AAD	Absolute average deviation	COP	Performance coefficient
EoS	Equation of state	GWP	Global warming potential
HFC	Hydrofluorocarbons	HFO	Hydrofluoroolefin
HTHP	High temperature heat pump	PR	Peng-Robinson

1. Introduction

As part of the effort to reduce energy consumption and to increase the efficiency of processes, Organic Rankine Cycles (ORC) and High Temperature Heat Pumps (HTHP) are two systems that can exploit and valorize low temperature waste heat sources. As usually waste heat is recoverable from 200°C and above, ORCs and HTHPs, using refrigerants as mediums, can increase the temperature of lower sources and valorize it as electricity or as high temperature heat.

The selection of the working fluid is generally made by comparing the performance coefficient (COP) of the systems. Literature that have been trying to find the most suitable working fluid agree that there is not such think as a perfect fluid (Badr et al., 1985), (Rahbar et al., 2017) . To find the most suitable working fluid, models are used to compute the COP of the system which means that models need to be fitted with experimental data.

Among HFCs, HFC 245fa was often the working fluid of choice. Since f-gas regulations, there is a need for low GWP working fluid. It is usually a HFO type refrigerant that will replace HFC 245fa. But HFOs are often flammable where HFCs were not. This effect can be mitigated with HFO-HFC mixtures.

Hydrofluoroolefins are being investigated (in pure form or mixtures) as HFC alternatives since the f gas regulation from 2015. R1336mzz(E) is among the HFO of great interest. As for the major part of HFOs, experimental data for R1336mzz(E) are still scarce and needed to evaluate both ORC and HTHP cycles performances. As such, it is expected to be of great interest both in ORCs and in HTHPs not only under its pure form but also in mixtures.

The temperature glide, inherent to zeotropic mixtures, is a good match to the temperature evolution of the heat source. They are particularly well suited for systems like ORCs where a non-isothermal phase transition at constant pressure occurs (Chys et al., 2012), or for HTHPs where they can replace pure fluid

transcritical systems (Besbes et al., 2014). As a result, exergetic losses are reduced as well as irreversibilities, improving overall performances of the system.

In order to evaluate temperature glide, It is important to study the phase equilibrium properties and to evaluate the phase diagram of such mixtures.

We studied 5 differents working fluids in combination with the R1336mzz(E); one hydrocarbon (R290), three HFCs (R152a, R227ea, R134a) and one HFO (R1234ze(E)).

In this work, isothermal vapor-liquid equilibria (VLE) data were measured with an in-house apparatus which technique is based on static-analytic method (Coquelet et al., 2019). Data obtained were correlated with the Peng-Robinson cubic Equation of State (Peng and Robinson, 1976) (PR EoS) associated to a Mathias-Copeman alpha function (Mathias and Copeman, 1983) and classical mixing rule.

2. Experimental section

2.1 Materials. In table 1 we list the suppliers of the chemicals and associated purities. No further purification was performed but a degassing was carried out.

Table 1 : Purities and suppliers of refrigerants.

Chemicals	CAS number	Purity (vol%)	Analysis method	Supplier
Propane	74-98-6	99.95	GC	MESSER
R134a	811-97-2	99.50	GC	Climalife
R152a	75-37-6	99.80	GC	Inventec
R227ea	431-89-0	99.50	GC	Climalife
R1234ze(E)	29118-24-9	99.50	GC	Climalife
R1336mzz(E)	66711-86-2	99.99	GC	Chemours

GC : Gas chromatograph

2.2 Experimental apparatus. The apparatus used in this work is presented in Figure 1 and is similar as the one used by Juntarachat et al (Juntarachat et al., 2014).

An equilibrium cell is immersed in a thermo-regulated liquid bath (LAUDA RP 3530) with a temperature control within 0.01K. In order to perform accurate measurement of temperature, two platinum resistance thermometer probes (Pt100) are inserted inside wells drilled directly into the top and bottom flanges of the equilibrium cell. They are connected to an HP data acquisition unit (Agilent 34970A). These two Pt100 are carefully and periodically calibrated against a 25Ω reference platinum resistance thermometer (PT25 – Hart Scientific) which is calibrated by the Laboratoire National d'Essais (Paris, France) based on the 1990 International Temperature Scale (ITS 90). The resulting combined uncertainty of temperature measurements is 0.03K.

Pressure in the cell is measured with a pressure transducer (DRUCK, model PTX 611, range 0-6MPa) connected to the same Agilent data acquisition unit as the two Pt100. The pressure transducer is maintained at constant temperature (higher than the highest temperature of study) by means of heating cartridge, controlled by a PID regulator (WEST Instruments, model 6100+). The pressure transducer was

calibrated against a pressure automated calibrator (GE Sensing, model PACE 5000). The combined uncertainty in the pressure measurements is estimated to be 1 kPa.

The Agilent online data acquisition system is connected to a personal computer through a RS-232 interface. This complete system allows real time readings and recording of temperatures and pressures all along the different isothermal runs.

The analytical analysis were carried out using two pneumatic samplers ROLSI^{TM} connected to a gas chromatograph (PERICHROM Model PR2100) equipped with a thermal conductivity detector (TCD) connected to a data acquisition system (WINILAB III). The analytical column is a 5% Krytox on CarboBlackB 60/80 mesh (silcosteel tube, length 2m, diameter 1/8 in). The TCD was repeatedly calibrated by introducing known amount of each pure compound using an automatic syring (model eVOL from SGE) in the injector of the gas chromatograph. Taking into account the uncertainties due to calibration and the dispersion of analyses, accuracy on vapor and liquid mole number fractions is estimated to be 1.5% at maximum, therefore the maximum extended uncertainty on the molar fractions is U(x/y, k=2) = 0.003, over the whole range of concentration.

Uncertainties on pressure and temperature are calculated so that:

$$u(T) = \sqrt{u^2{}_{rep}(T) + u^2{}_{cal}(T)} \quad (1)$$

With :

$$u_{cal}(T) = \frac{\max(\Delta T)}{\sqrt{3}} \quad (2)$$

And so:

$$u(P) = \sqrt{u^2{}_{rep}(P) + u^2{}_{cal}(P)} \quad (3)$$

$$u_{cal}(P) = \frac{\max(\Delta P)}{\sqrt{3}} \quad (4)$$

While uncertainties of composition are defined by:

$$u(x) = \sqrt{u^2{}_{rep} + u^2{}_{cal} + u^2{}_{purity1} + u^2{}_{purity2}} \quad (5)$$

With :

$$u_{cal}(x) = \sqrt{\left(\frac{\partial x_1}{\partial n_1}\right)^2 u^2(n_1) + \left(\frac{\partial x_1}{\partial n_2}\right)^2 u^2(n_2)} \quad (6)$$

$$u_{purity} = \frac{1-p}{\sqrt{3}} \quad (7)$$

2.3 Experimental procedure. At room temperature, the equilibrium cell and its loading lines are evacuated down to 0.1 Pa. One gas cylinder is loaded with R1336mzz(E) (C_1) and the second with another refrigerant (C_2). At the required equilibrium temperature (equilibrium temperature is assumed to be reached when the two Pt100 give the same temperature value within their temperature uncertainty for at least 10 min), a volume of about 5cm^3 of R1336mzz(E) is introduced into the equilibrium cell. The vapor pressure of the heaviest component (R1336mzz(E)) is then recorded at this temperature. To describe the two-phase envelope with at least 10 twin points (liquid and vapor), given amounts of the light component (other refrigerant) are introduced step by step, leading to successive equilibrium mixtures. Equilibrium is assumed when the total pressure remains unchanged within ± 1.0 kPa during a period of 10 minutes under efficient stirring.

For each equilibrium condition, at least 5 samples of both vapor and liquid phases are withdrawn using the pneumatic samplers ROLSI^{TM} and analyzed in order to check for measurement repeatability.

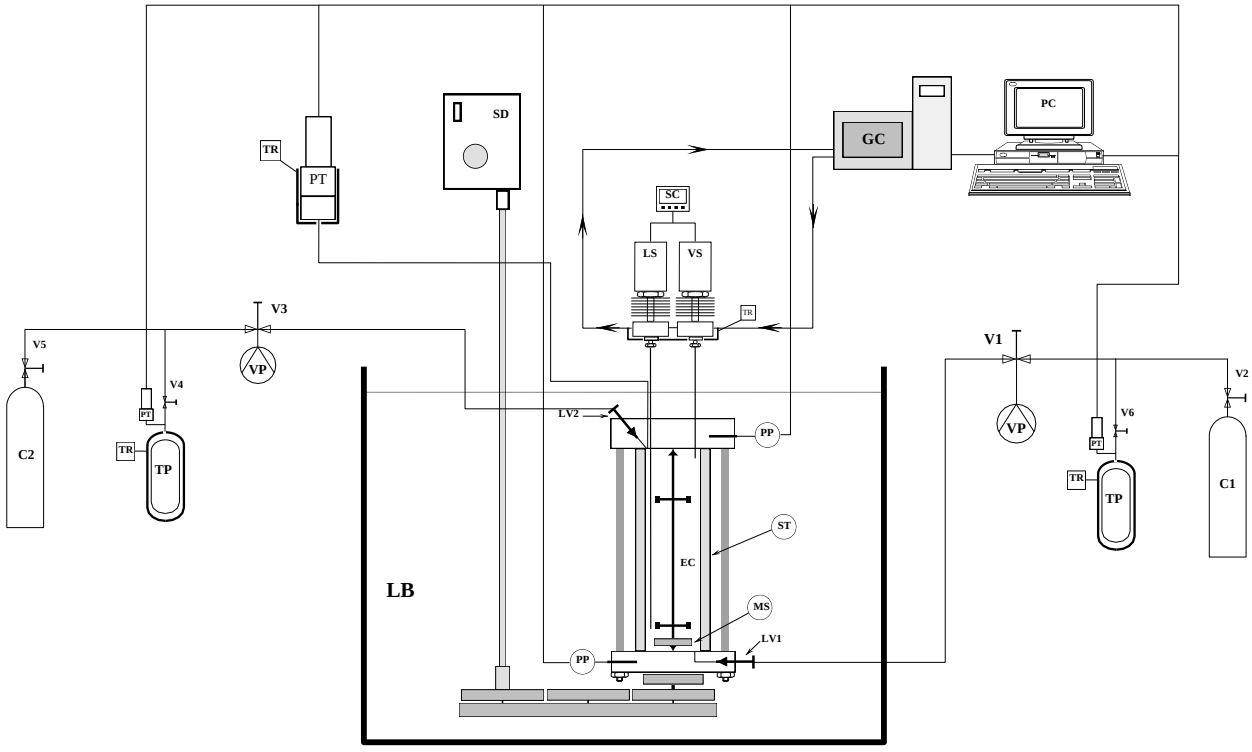

Figure 1 : Schematic diagram of the static-analytic apparatus. (C1) More volatile compound. (C2) Less-volatile compound. (EC) Equilibrium cell. (GC) Gas chromatograph. (LB) Liquid bath. (LS) Liquid sampler. (LV) Loading valve. (MS) Magnetic stirrer. (PC) Personal computer. (PP) Platinum resistance thermometer probe. (PT) Pressure transducer. (SC) Sample control. (SD) Stirring device. (ST) Saphhire tube. (TP) Thermal press. (TR) Temperature regulator. (Vi) Valve. (VP) Vacuum pump. (VS) Vapor sampler.

3. Modeling

The approach used is a Peng-Robinson equation of state (PR-EoS) combined with the van der Waals mixing rules and Mathias-Copeman alpha function for the modeling of pure fluids :

$$P = \frac{RT}{v-b} - \frac{a(T)}{v(v+b)+b(v-b)} \qquad (8)$$

Where *T*, *P* and *v* are respectively the temperature, pressure and molar volume of the system. The parameters *a* and *b* are given by :

$$b = 0.07780\frac{RT_C}{P_C} \quad (9)$$

$$a(T) = a_C\alpha(T) \quad (10)$$

Where :

$$a_C = 0.45724\frac{(RT_C)^2}{P_C} \quad (11)$$

And *α(T)* is a Mathias-Copeman alpha function given by :

$$\alpha(T) = \left[1 + \sum_{i=1}^{i=3} m_i\left(1 - \sqrt{\frac{T}{T_C}}\right)^i\right]^2 \quad (12)$$

Where m_1, m_2 and m_3 are three adjustable parameters. Pure component properties are presented in Table 2. Mathias-Copeman coefficients were adjusted on literature data for the whole temperature domain (278K to 403K) using a modified simplex algorithm which objective function is defined by:

$$F = \frac{100}{N}\sum\left(\frac{P_{exp}-P_{calc}}{P_{exp}}\right)^2 \quad (13)$$

Where *N* is the number of data points, P_{exp} is the measured pressure, and P_{calc} is the calculated pressure. For mixtures, the van der Waals mixing rules are applied with a binary interaction parameter k_{ij}. The expression for *a* and *b* becomes :

$$a = \sum_i\sum_j x_i x_j a_{ij} \quad (14)$$

$$a_{ij} = \sqrt{a_i a_j}\left(1 - k_{ij}\right) \quad (15)$$

$$b = \sum_i x_i b_i \quad (16)$$

Where x_i, x_j are the mole fractions of component *i* and *j* and a_i, a_i and b_i, b_j are the pure fluids parameters of component *i* and *j*. This Peng-Robinson model was used with a classical flash algorithm.

Binary interaction parameters k_{ij} were adjusted on experimental data using the objective function :

$$F = \frac{100}{N}\left[\sum_1^N\left(\frac{x_{exp}-x_{calc}}{x_{exp}}\right)^2 + \sum_1^N\left(\frac{y_{exp}-y_{calc}}{y_{exp}}\right)^2\right] \quad (17)$$

4. Results

4.1 Pure components

Table 2 presents critical temperature and pressure, as well as acentric factors for all considered refrigerants.

Table 2 : Critical parameters and acentric factors of refrigerants. Values from REFPROP 10.0, [a] Tanaka et al (Tanaka et al., 2017).

Component	*Tc* (K)	*Pc* (MPa)	
			ω
R1336mzz(E)[a]	403.37	2.7664	0.4053
R134a	374.21	4.0593	0.32684
R152a	386.41	4.5168	0.27521
R227ea	374.90	2.9250	0.357
R1234ze(E)	382.51	3.6349	0.313
R290	369.95	4.2455	0.152

Table 3 presents the adjusted parameters for the Mathias-Copeman α-function, reproducing vapor pressures within 1% deviation.

Table 3 : Mathias Copeman parameters of refrigerants. [b] this work data, [c] data from DIPPR (Component+), [d] Valtz et al (Valtz et al., 2004), [e]data generated with REFPROP 10.0 (293K to 380K).

Component				AAD (%)	BIAS (%)
	m_1	m_2	m_3		
R1336mzz(E)[b]	0.9801	-0.3961	1.5561	0.02	0.02
R134a[c]	0.8498	0.0066	-0.0536	0.8	0.7
R152a[c]	0.8345	-0.6312	0.7901	0.2	-0.03
R227ea[d]	0.8982	-0.1631	0.7295	0.4	0.3
R1234ze(E)[e]	0.8852	-1.0253	4.6541	0.06	0.01
R290[c]	0.6001	-0.0063	0.1739	0.7	-0.5

Table 4 presents the experimental vapor pressure of R1336mzz(E), measured in this work. Figure 2a shows a comparison of these data against the data measured by Tanaka et al, 2017, and the Peng-Robinson model. Figure 2b shows that measured vapor pressures follow the linearity between $\ln(P^s)$ and $1/T$ as described by Clapeyron's relation.

Table 4 : Experimental results of saturation pressure of HFO – 1336mzz(E)

T (K)	*P* (MPa)	*T* (K)	*P* (MPa)
278.18	0.091	322.43	0.424
283.10	0.112	327.34	0.488
288.01	0.135	332.24	0.559
292.93	0.162	337.15	0.638
297.85	0.193	342.05	0.725
302.77	0.229	346.96	0.820
307.68	0.269	351.86	0.925
312.61	0.314	356.73	1.039
317.51	0.366		

U(T, k=2) = 0.03K, U(P, k=2) =0.001 MPa

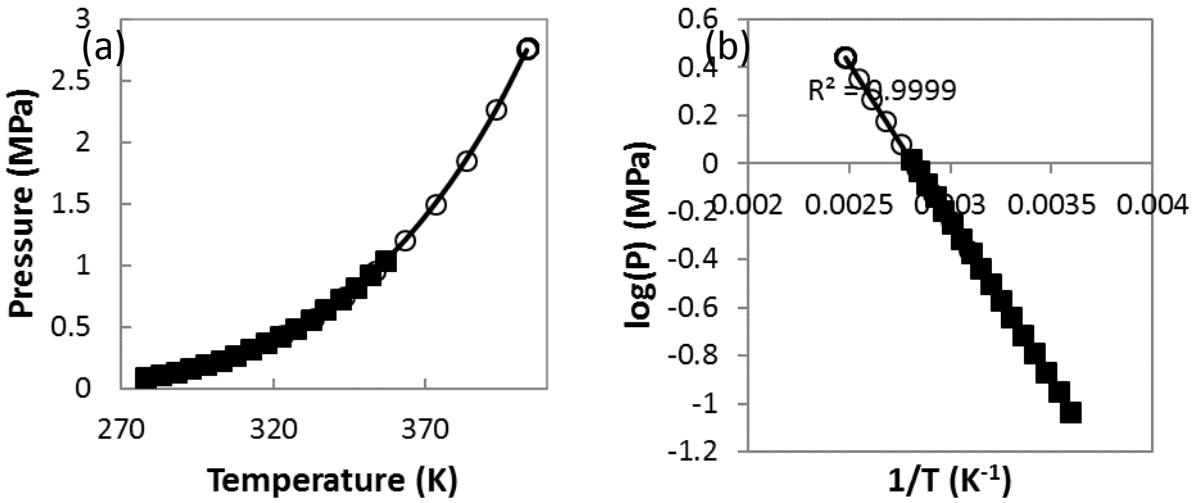

Figure 2 : Comparison of experimental vapor pressures for HFO – 1336mzz(E) between this work: ■, Tanaka et al, 2017 : ○ and Peng-Robinson: solid line.

4.2 Mixtures

Table 5 presents k_{ij} parameters for each couple and each temperature, along with the k_{ij} without temperature dependence. Experimental results are presented in table 6 to 10, with the PR model results (using temperature-dependend k_{ij}). Combined expanded uncertainties on liquid and vapor fractions are also displayed as well as the absolute deviation between calculated and measured data.

Data from tables 6 to 10 are plotted in figures 3 to 7. Mean BIAS and mean absolute deviation (calculated with equations 18 and 19) are presented in table 11.

Figures 8 to 12 show the relative volatility against the liquid fraction of the more volatile refrigerant.

Table 5 : Temperature dependant binary interaction parameters k_{ij} of refrigerants mixtures.

R1336mzz(E)-…	**R290**	**R134a**	**R152a**	**R227ea**	**R1234ze(E)**
313 K	0.117	0.0282	0.0263	0.0102	0.00784
333 K	0.116	0.0310	0.0260	0.0105	0.00993
353 K	0.121	0.0290	0.0270	0.00950	0.0106
Without T dependance	0.118	0.0290	0.0268	0.0100	0.00984

a) R290-R1336mzz(E)

Table 6: Experimental VLE data of the R290 (1) / R1336mzz(E) (2) system.

Experimental data							Calculated data			
P_{exp} /MPa	N_x	$x_{1,exp}$	U(x)	N_y	$y_{1,exp}$	U(y)	$x_{1,calc}$	$y_{1,calc}$	dx	dy
					313.19 K					
0.4632	6	0.066	0.001	5	0.311	0.004	0.067	0.320	0.001	0.009
0.6160	9	0.147	0.002	5	0.496	0.004	0.149	0.505	0.002	0.009
0.7880	9	0.259	0.005	6	0.624	0.004	0.256	0.633	0.003	0.009
0.9985	5	0.438	0.004	5	0.737	0.005	0.427	0.742	0.011	0.005
1.1965	7	0.670	0.004	7	0.823	0.002	0.658	0.831	0.012	0.008
1.3021	11	0.830	0.002	7	0.891	0.002	0.826	0.894	0.004	0.003
					333.15 K					
0.8449	7	0.097	0.001	10	0.326	0.004	0.101	0.334	0.004	0.008
1.1451	5	0.227	0.002	5	0.518	0.004	0.230	0.531	0.003	0.013
1.4373	6	0.382	0.004	6	0.645	0.004	0.382	0.656	0.000	0.011
1.7468	13	0.591	0.004	5	0.757	0.002	0.588	0.765	0.003	0.008
2.0167	6	0.836	0.002	6	0.881	0.002	0.829	0.880	0.007	0.001
					353.08 K					
1.4567	6	0.148	0.002	7	0.344	0.004	0.149	0.352	0.001	0.008
1.9362	7	0.316	0.004	5	0.528	0.004	0.315	0.536	0.001	0.008
2.2302	5	0.436	0.004	7	0.616	0.004	0.434	0.621	0.002	0.005
2.5472	6	0.580	0.004	8	0.702	0.003	0.578	0.707	0.002	0.005
2.7350	7	0.681	0.004	6	0.763	0.003	0.673	0.761	0.008	0.002

U(T, k=2) =0.03 K, U(P, k = 2) = 0.001 MPa

Table 7 : Experimental VLE data of the R134a (1) / R1336mzz(E) system.

Experimental data							Calculated data			
P_{exp} /MPa	N_x	$x_{1,exp}$	$U(x)$	N_y	$y_{1,exp}$	$U(y)$	$x_{1,calc}$	$y_{1,calc}$	dx	dy
					313.24 K					
0.4306	7	0.129	0.006	6	0.308	0.006	0.134	0.326	0.005	0.018
0.5288	6	0.252	0.012	6	0.500	0.006	0.261	0.511	0.009	0.011
0.6327	7	0.403	0.007	6	0.649	0.006	0.403	0.652	0.000	0.003
0.7222	8	0.534	0.007	5	0.748	0.006	0.532	0.747	0.002	0.001
0.8337	5	0.695	0.007	7	0.848	0.006	0.701	0.847	0.006	0.001
0.8985	8	0.805	0.006	5	0.904	0.006	0.804	0.900	0.001	0.004
					333.19 K					
0.7358	5	0.125	0.006	6	0.270	0.006	0.130	0.285	0.005	0.015
0.9109	5	0.271	0.007	5	0.477	0.006	0.276	0.487	0.005	0.010
1.1194	5	0.458	0.011	5	0.659	0.006	0.458	0.659	0.000	0.000
1.3115	6	0.633	0.007	5	0.789	0.006	0.633	0.783	0.000	0.006
1.5086	6	0.824	0.006	5	0.904	0.006	0.821	0.896	0.003	0.008
					353.12 K					
1.2292	6	0.151	0.006	5	0.278	0.006	0.160	0.292	0.009	0.014
1.4885	5	0.303	0.006	5	0.471	0.006	0.312	0.479	0.009	0.008
1.8177	5	0.504	0.006	5	0.657	0.006	0.507	0.656	0.003	0.001
2.0626	6	0.655	0.006	6	0.772	0.006	0.652	0.765	0.003	0.007
2.3279	7	0.817	0.006	5	0.873	0.006	0.810	0.872	0.007	0.001

U(T, k = 2) = 0.03 K, U(P, k = 2) =0.001 MPa

Table 8 : Experimental VLE data of the R152a (1) / R1336mzz(E) system.

Experimental data							Calculated data			
P_{exp} /MPa	N_x	$x_{1,exp}$	U(x)	N_y	$y_{1,exp}$	U(y)	$x_{1,calc}$	$y_{1,calc}$	dx	dy
					313.21 K					
0.4022	6	0.100	0.003	5	0.241	0.003	0.110	0.268	0.010	0.027
0.501	7	0.245	0.004	6	0.467	0.003	0.252	0.484	0.007	0.017
0.5981	5	0.397	0.005	4	0.619	0.003	0.401	0.636	0.004	0.017
0.6990	7	0.577	0.003	5	0.760	0.003	0.572	0.760	0.005	0.000
0.7991	5	0.766	0.003	5	0.873	0.003	0.760	0.868	0.006	0.005
					333.15 K					
0.7296	6	0.138	0.003	6	0.279	0.003	0.146	0.293	0.008	0.014
0.9031	7	0.306	0.004	7	0.500	0.003	0.314	0.511	0.008	0.011
1.0465	9	0.457	0.009	9	0.642	0.003	0.461	0.648	0.004	0.006
1.2060	7	0.636	0.003	5	0.775	0.003	0.636	0.775	0.000	0.000
1.3568	5	0.815	0.003	5	0.889	0.003	0.816	0.887	0.001	0.002
					353.08 K					
1.2580	6	0.190	0.003	5	0.322	0.003	0.201	0.336	0.011	0.014
1.4060	5	0.289	0.003	5	0.443	0.003	0.300	0.455	0.011	0.012
1.6752	1	0.476	0.003	6	0.626	0.003	0.486	0.631	0.006	0.005
1.9696	7	0.701	0.003	5	0.794	0.003	0.701	0.794	0.000	0.000
2.1849	6	0.870	0.003	6	0.911	0.003	0.870	0.909	0.000	0.002

U(T, k = 2) = 0.03 K, U(P, k = 2) =0.001 MPa

Table 9 : Experimental VLE data of the R227ea (1) / R1336mzz(E) system.

	Experimental data						Calculated data			
P_{exp} /MPa	N_x	$x_{1,exp}$	U(x)	N_y	$y_{1,exp}$	U(y)	$x_{1,calc}$	$y_{1,calc}$	dx	dy
					313.22 K					
0.3771	6	0.140	0.006	8	0.245	0.007	0.138	0.250	0.002	0.005
0.4269	5	0.272	0.007	10	0.421	0.007	0.264	0.421	0.008	0.000
0.4937	5	0.444	0.007	4	0.604	0.007	0.438	0.604	0.006	0.000
0.5818	6	0.675	0.007	4	0.792	0.006	0.674	0.793	0.001	0.001
0.6291	6	0.799	0.006	5	0.878	0.006	0.802	0.879	0.003	0.001
					333.18 K					
0.6857	6	0.185	0.006	6	0.286	0.007	0.181	0.288	0.004	0.002
0.7475	7	0.287	0.007	5	0.411	0.007	0.282	0.413	0.005	0.002
0.8252	6	0.414	0.007	6	0.547	0.007	0.411	0.549	0.003	0.002
0.9168	6	0.566	0.007	7	0.684	0.007	0.564	0.686	0.002	0.002
1.056	6	0.797	0.006	7	0.863	0.006	0.798	0.864	0.001	0.001
					353.11 K					
1.1029	7	0.168	0.006	5	0.243	0.007	0.168	0.247	0.000	0.004
1.2474	11	0.332	0.007	6	0.434	0.007	0.330	0.436	0.002	0.002
1.398	6	0.502	0.007	7	0.602	0.007	0.499	0.601	0.003	0.001
1.5417	7	0.660	0.007	5	0.737	0.007	0.657	0.738	0.003	0.001
1.7099	6	0.841	0.006	6	0.878	0.006	0.839	0.880	0.002	0.002

U(T, k = 2) = 0.03 K, U(P, k = 2) =0.001 MPa

Table 10 : Experimental VLE data of the R1234ze(E) (1) / R1336mzz(E) system.

Experimental data							Calculated data			
P_{exp} /MPa	N_x	$x_{1,exp}$	U(x)	N_y	$y_{1,exp}$	U(y)	$x_{1,calc}$	$y_{1,calc}$	dx	dy
					313.21 K					
0.394	6	0.158	0.006	5	0.285	0.006	0.154	0.286	0.004	0.001
0.4744	8	0.336	0.006	6	0.514	0.006	0.333	0.516	0.003	0.002
0.5301	5	0.460	0.006	6	0.639	0.006	0.459	0.639	0.001	0.000
0.6399	6	0.705	0.007	7	0.830	0.006	0.708	0.829	0.003	0.001
0.6961	5	0.830	0.006	6	0.907	0.006	0.837	0.909	0.007	0.002
					333.18 K					
0.7065	8	0.187	0.006	6	0.302	0.006	0.185	0.305	0.002	0.003
0.8206	6	0.350	0.006	5	0.500	0.006	0.347	0.500	0.003	0.000
0.9308	8	0.506	0.007	6	0.650	0.006	0.505	0.651	0.001	0.001
1.0315	7	0.648	0.006	5	0.768	0.006	0.649	0.767	0.001	0.001
1.1683	5	0.841	0.006	7	0.902	0.006	0.846	0.903	0.005	0.001
					353.13 K					
1.1532	9	0.194	0.006	5	0.286	0.006	0.193	0.290	0.001	0.004
1.3231	5	0.359	0.006	6	0.478	0.006	0.358	0.479	0.002	0.001
1.4874	5	0.516	0.006	6	0.631	0.006	0.515	0.630	0.001	0.001
1.6976	5	0.713	0.008	7	0.796	0.006	0.715	0.794	0.002	0.002
1.8721	6	0.872	0.006	5	0.912	0.006	0.877	0.914	0.005	0.002

U(T, k = 2) = 0.03 K, U(P, k = 2) =0.001 MPa

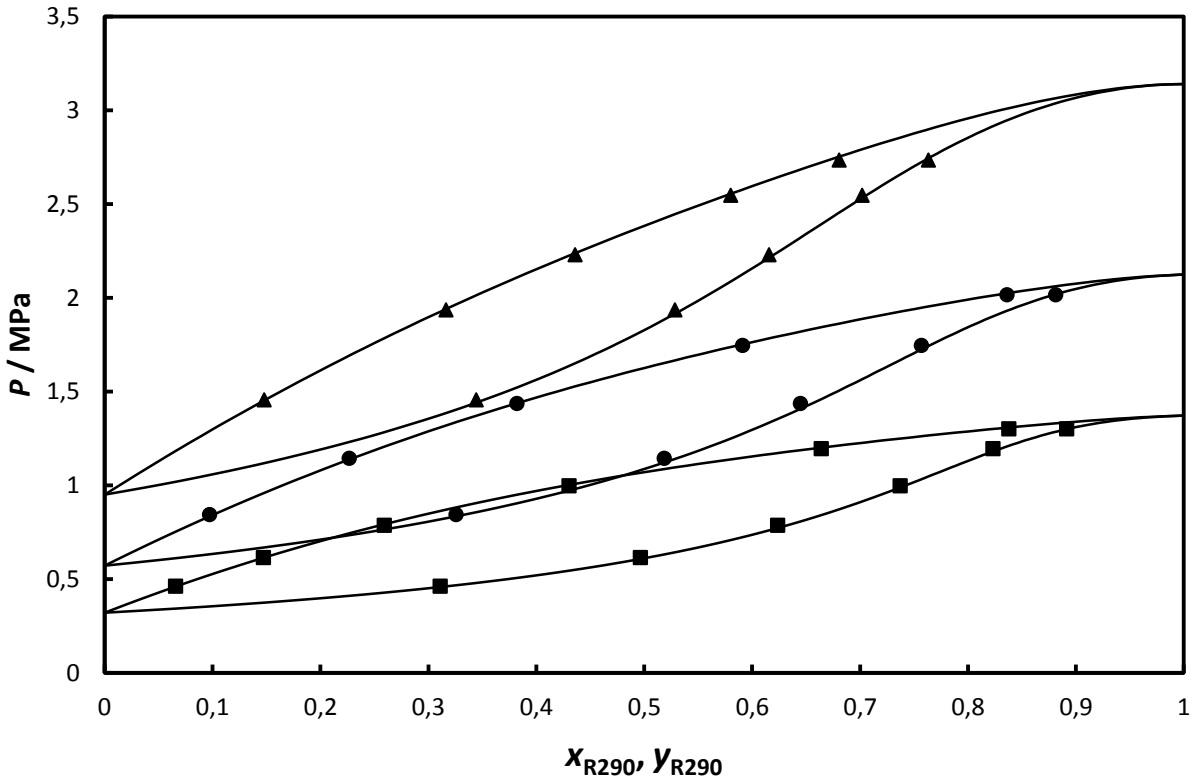

Figure 3 : Phase diagram for the R290 (1) / R1336mzz(E) (2) binary system. (■) 313.19K, (●) 333.15 K , (▲) 353.08 K, (solid line): Peng-Robinson EoS with parameters presented in table 5.

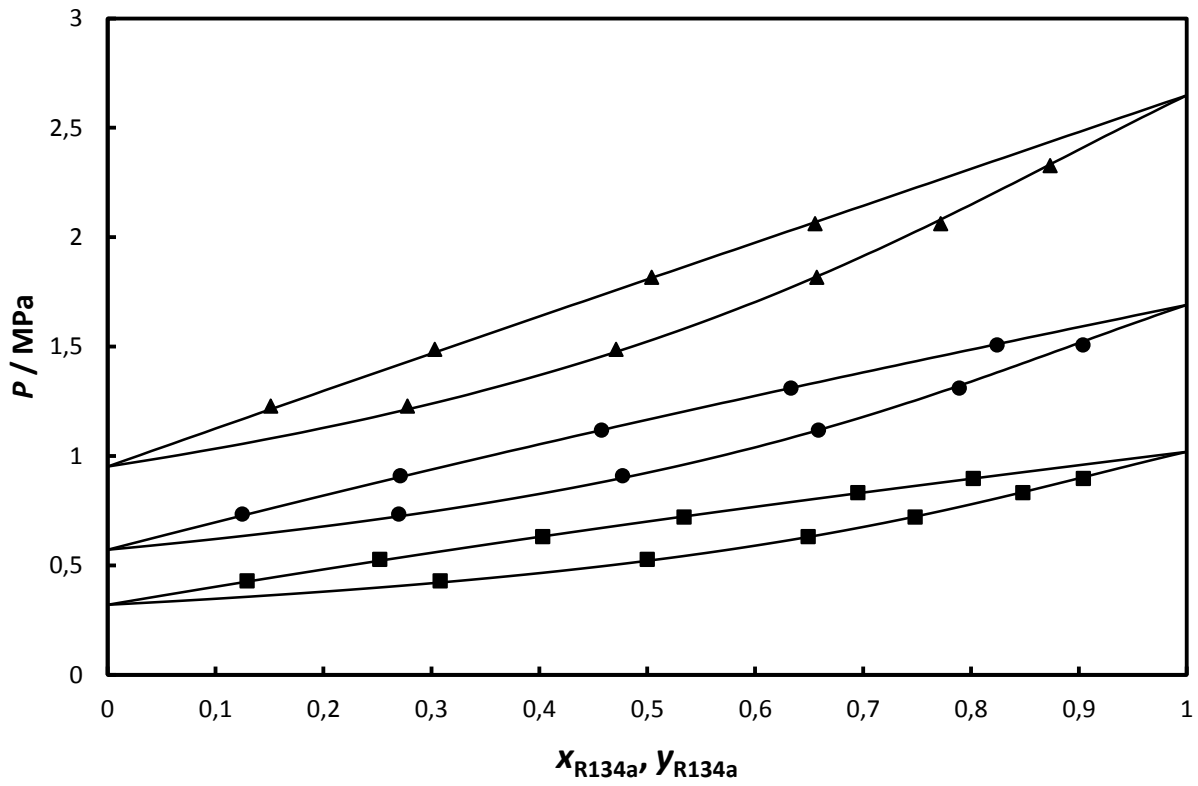

Figure 4 : Phase diagram for the R134a (1) / R1336mzz(E) (2) system. (■) 313.24K, (●) 333.19K, (▲) 353.12 K, (solid line) Peng-Robinson model EoS with parameters presented in table 5.

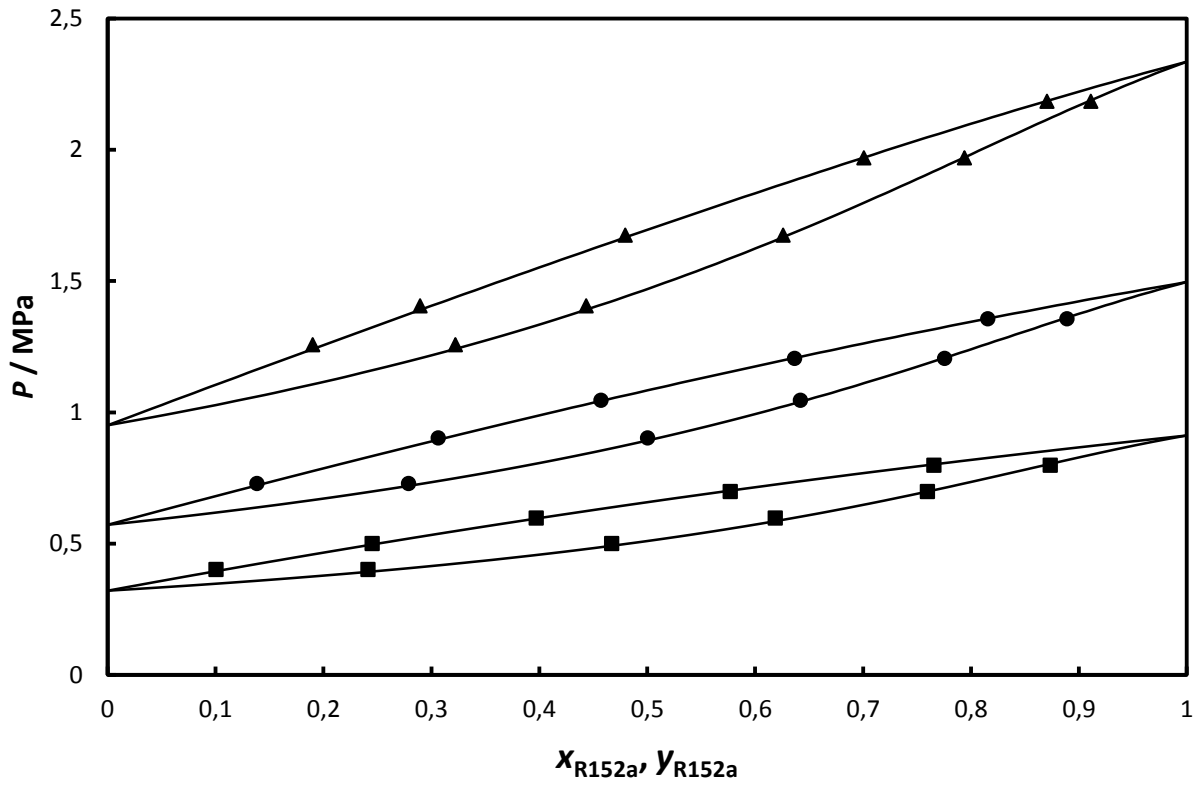

Figure 5: Phase diagram for the R152a (1) / R1336mzz(E) (2) system. (■) 313.21K, (●) 333.15K, (▲) 353.08K, (solid line) Peng-Robinson model EoS with parameters presented in table 5.

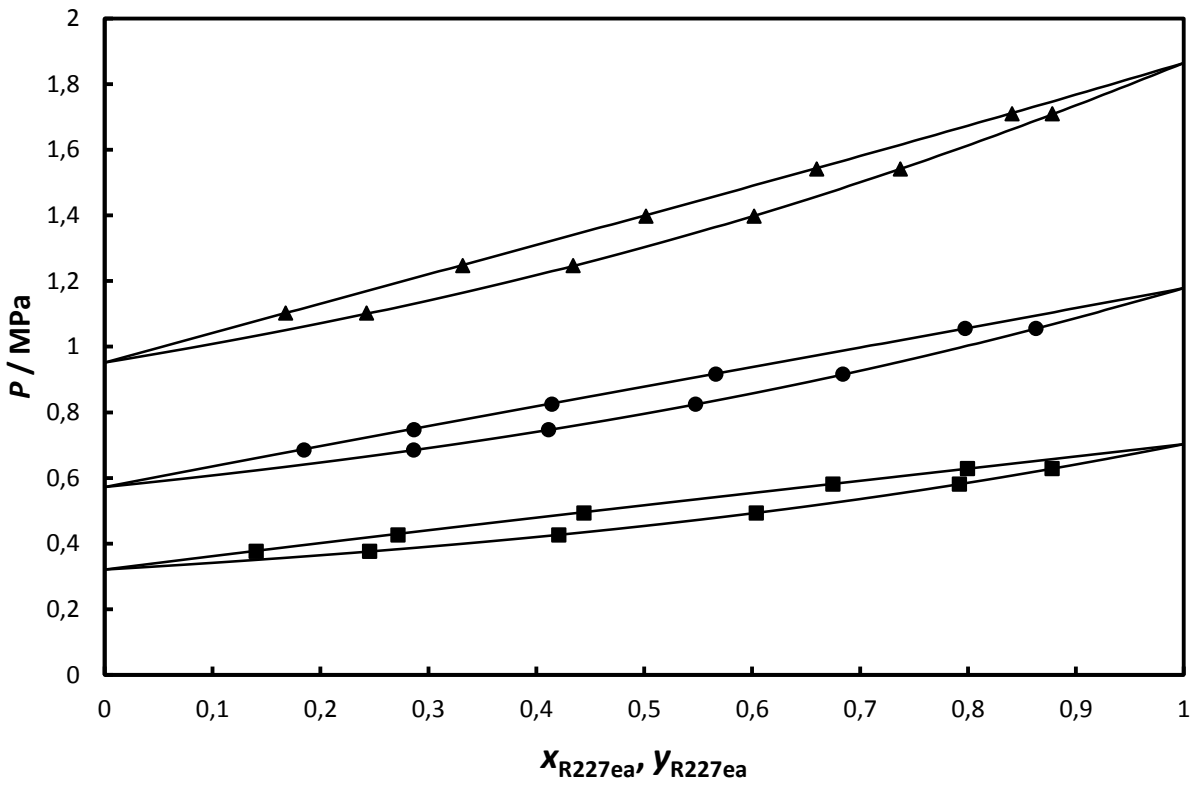

Figure 6: Phase diagram for the R227ea (1) / R1336mzz(E) (2) system. (■) 313.22K, (●) 333.18K, (▲) 353.11K, (solid line) Peng-Robinson model EoS with parameters presented in table 5.

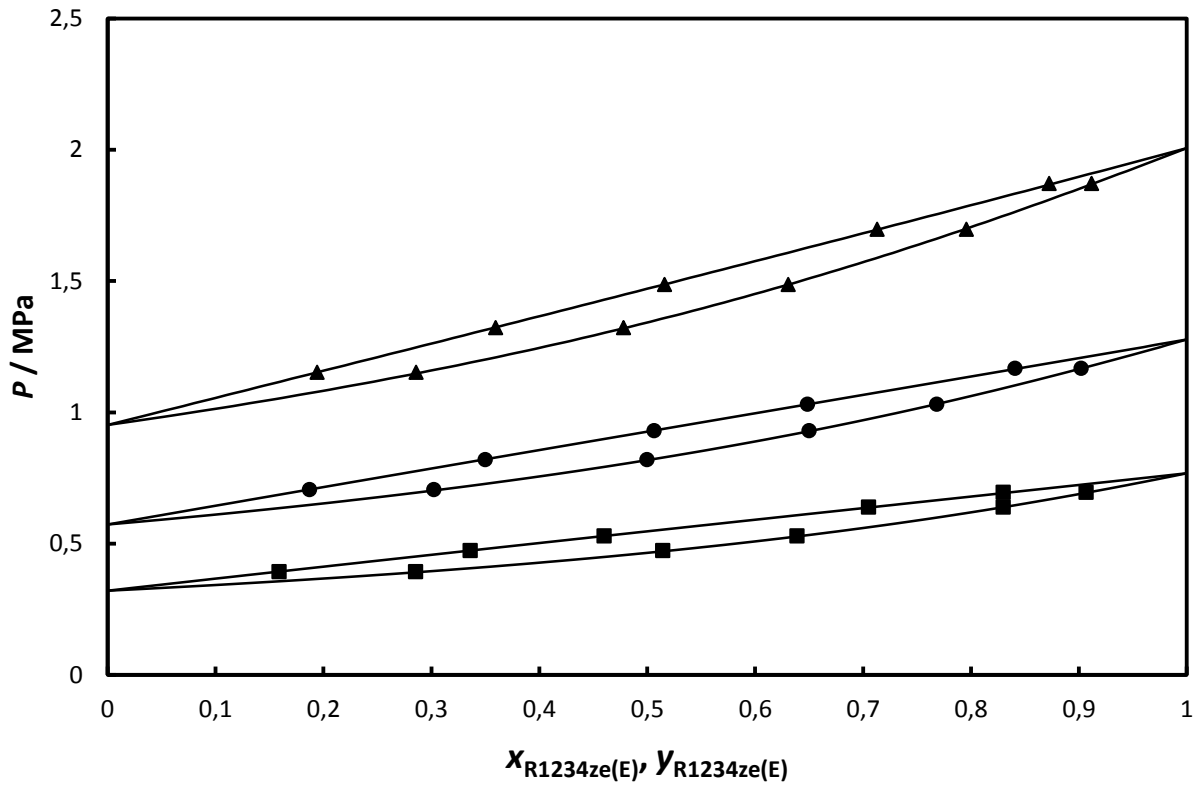

Figure 7: Phase diagram for the R1234ze(E) (1) / R1336mzz(E) (2) system. (■) 313.21 K, (●) 333.18K, (▲) 353.13K., (solid lines) Peng-Robinson model EoS with parameters presented in table 5.

Table 11 : AAD and BIAS between experimental measurements and modeling.

T(K)	BIAS X (%)	BIAS Y(%)	AAD X (%)	AAD Y (%)
		Propane / R1336mzz(E)		
313.19	0.1	-1.3	1.7	1.3
333.15	-0.8	-1.6	1.4	1.6
353.08	0.3	-1.0	0.7	1.1
No T dep.	-0.05	-1.3	1.3	1.4
		R134a / R1336mzz(E)		
313.24	-1.3	-1.3	1.5	1.5
333.19	-1.3	-1.2	1.4	1.9
353.12	-1.7	-1.1	2.2	1.6
No T dep.	-1.6	-1.3	2.0	1.7
		R152a / R1336mzz(E)		
313.21	-2.4	-3.4	3.0	3.6
333.15	-1.8	-1.6	1.8	1.7
353.08	-2.2	-1.5	2.2	1.6
No T dep.	-1.8	-2.0	2.2	2.3
		R227ea/R1336mzz(E)		
313.22	1.1	-0.4	1.2	0.4

333.18	0.9	-0.4	0.9	0.4
353.11	0.3	-0.5	0.4	0.5
No T dep.	0.7	-0.5	0.8	0.5
		R1234ze(E) / R1336mzz(E)		
313.21	0.5	-0.2	1.0	0.2
333.18	0.3	-0.3	0.6	0.3
353.13	0.1	-0.3	0.4	0.4
No T dep.	0.6	-0.1	0.9	0.5

$$AAD(\%) = \frac{100}{N}\sum\frac{|X_{calc}-X_{exp}|}{X_{exp}} \quad (18)$$

$$BIAS(\%) = \frac{100}{N}\sum\frac{X_{calc}-X_{exp}}{X_{exp}} \quad (19)$$

Where *X* is either the liquid or vapor fraction.

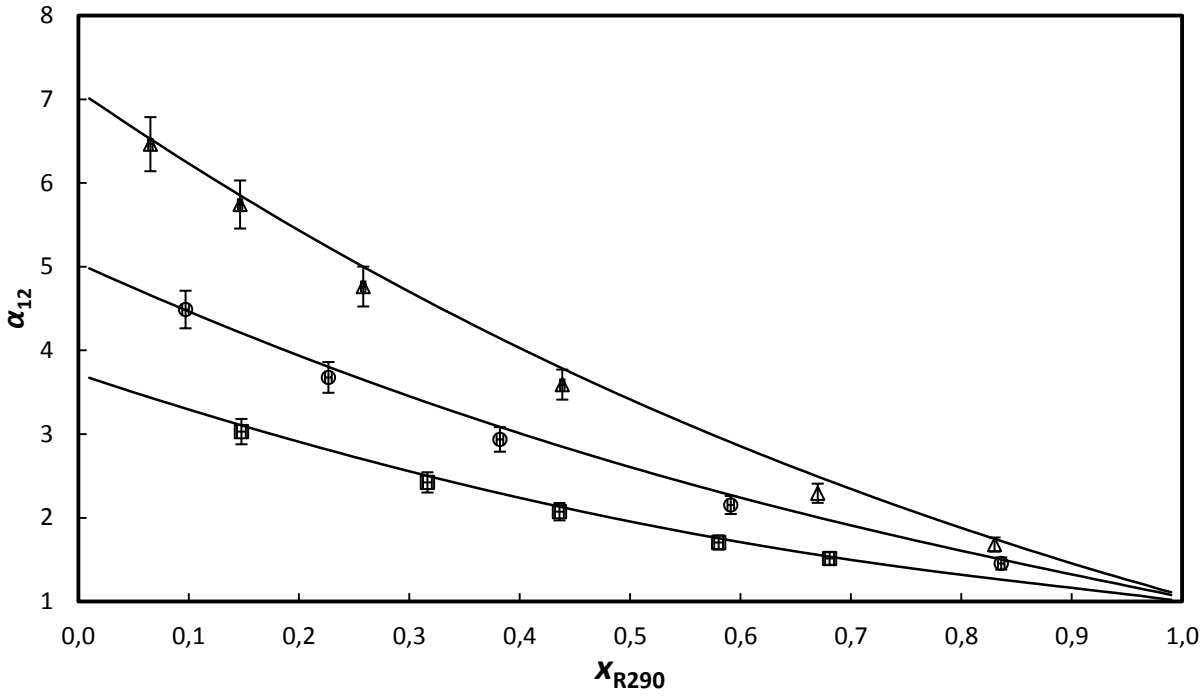

Figure 8 : Relative volatility of R290 – R1336mzz(E). □ 313.19K, ○ 333.15K, △ 353.08K, (solid line) Peng-Robinson model, error bar: 5%.

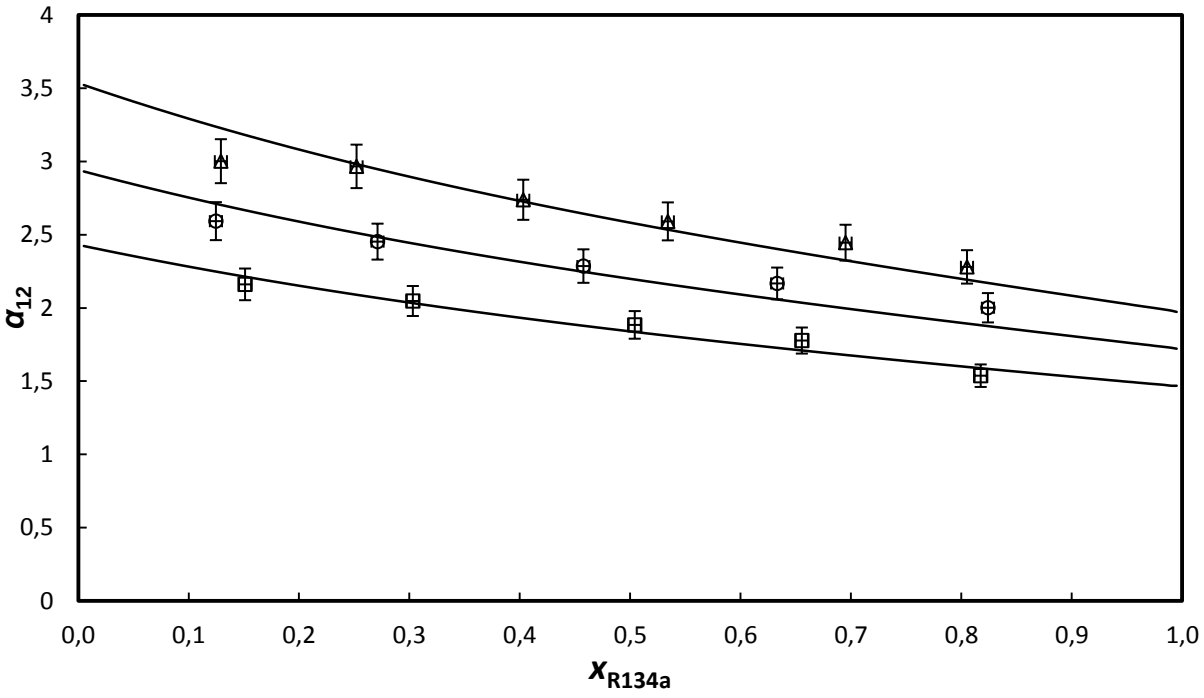

Figure 9 : Relative volatility of R134a – R1336mzz(E). □ 313.24K, ○ 333.19K, Δ 353.12K, (solid line) Peng-Robinson model, error bar : 5%.

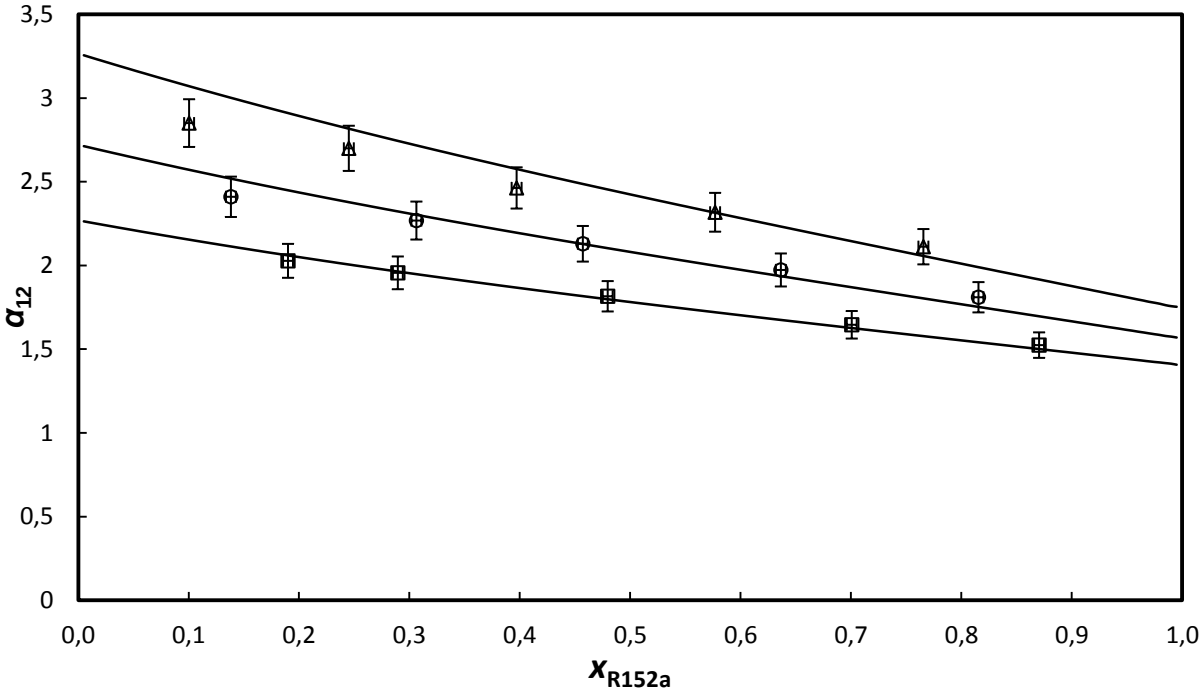

Figure 10 : Relative volatility of R152a – R1336mzz(E). □ 313.21K, ○ 333.15K, Δ 353.08K, (solid line) Peng-Robinson model, error bar : 5%.

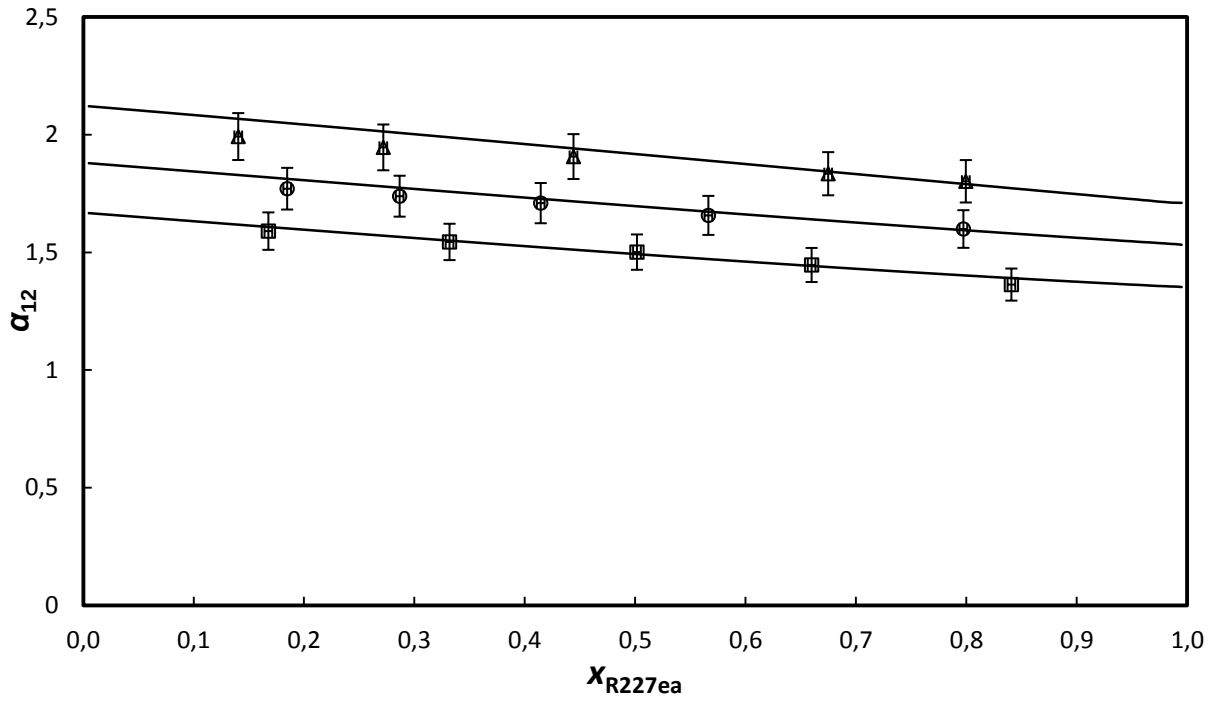

Figure 11 : Relative volatility of R227ea – R1336mzz(E). □ 313.22K, ○ 333.18K, △ 353.11K, (solid line) Peng-Robinson model, error bar: 5%.

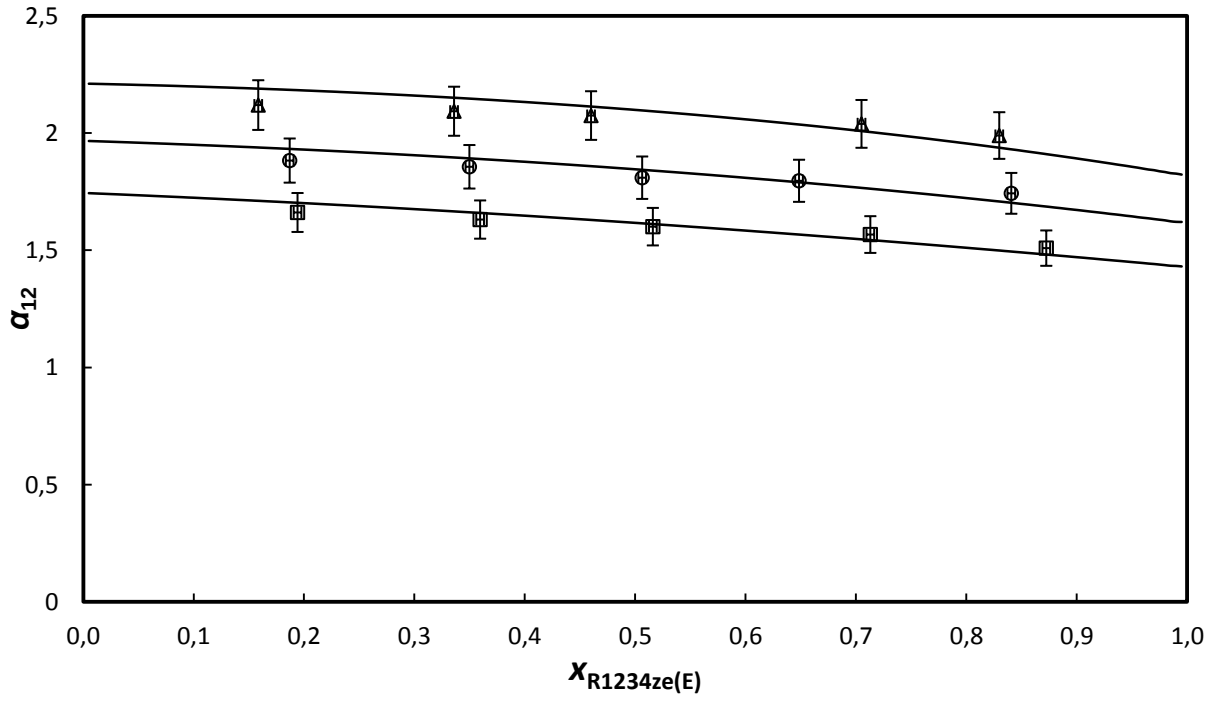

Figure 12 : Relative volativity of R1234ze(E) – R1336mzz(E) mixture. □ 313.21K, ○ 333.18K, △ 353.13K, (solid line) Peng-Robinson model, error bar: 5%.

5. Discussions

All of the binary couples are classified as Type I systems according to Konyneburg and Scott classification (Konynenburg and Scott, 1980). Figures 3 to 7 show a negative deviation from the ideal mixture behaviour for all systems. In particular, mixtures with R227ea and R1234ze(E) are nearly ideals. R290 – R1336mzz(E) mixture is the only system showing a difficulty to separates its components near pure propane composition. If an azeotropic behavior exists at temperatures under 313K, this system could be useful for refrigeration applications.

Relative volatility shows consistent data, as it is continuously decreasing, as shown in figures 8 to 12. The difficulty to separate the R290-R1336mzz(E) mixture into its pure components (near pure R1336mzz(E) compositions) can be seen as well on figure 8 (as well as on figure 3).

Though the model with a kij with no temperature dependence were not plotted, deviations and BIAS were provided in Table 11. For all of the systems, a model without temperature dependence for the interaction parameter is enough to get a good agreement between experimental and modeled data.

In a context of recuperation of the working fluid, it can be difficult to isolate both components (for the R290-R1336mzz(E) near pure propane composition).

In order to use fluids with a lesser GWP impact than HFCs, it could be useful to blend already used fluids with HFOs such as R1336mzz(E).

6. Conclusions

The data were successfully correlated with a Peng-Robinson model with a temperature dependant k_{ij}.

Measurements of the vapor-liquid equilibrium of 5 zeotropic mixtures were conducted. The data obtained were correlated within 5% of absolute error with a Peng-Robinson cubic equation of state associated with a Mathias-Copeman alpha function and van der Waals mixing rule. Measurements of the saturation pressure of the R1336mzz(E) were also conducted and are in good accordance with other results find in the literature.

Acknowledgement

The authors are grateful to Chemours and particularly Loïc CHEREAU for the sample of R1336mzz(E).

References

Badr, O., Probert, S.D., O'Callaghan, P.W., 1985. Selecting a working fluid for a Rankine-cycle engine. Appl. Energy 21, 1–42.

Besbes, K., Zoughaib, A., Carlan, F.D., Peureux, J.-L., 2014. Exergy Based Methodology for Optimized Integration of Heat Pumps in Industrial Processes. Int. Refrig. Air Cond. Conf.

Chys, M., van den Broek, M., Vanslambrouck, B., De Paepe, M., 2012. Potential of zeotropic mixtures as working fluids in organic Rankine cycles. Energy, Integration and Energy System Engineering, European Symposium on Computer-Aided Process Engineering 2011 44, 623–632.

Coquelet, C., Valtz, A., Theveneau, P., 2019. Experimental Determination of Thermophysical Properties of Working Fluids for ORC Applications, in: ORC for Waste Heat Recovery Applications.

Juntarachat, N., Valtz, A., Coquelet, C., Privat, R., Jaubert, J.-N., 2014. Experimental measurements and correlation of vapor–liquid equilibrium and critical data for the CO2 + R1234yf and CO2 + R1234ze(E) binary mixtures. Int. J. Refrig. 47, 141–152.

Konynenburg, P.H. van, Scott, R.L., 1980. Critical lines and phase equilibria in binary van der Waals mixtures. Phil Trans R Soc Lond A 298, 495–540.

Mathias, P.M., Copeman, T.W., 1983. Extension of the Peng-Robinson equation of state to complex mixtures: Evaluation of the various forms of the local composition concept. Fluid Phase Equilibria 13, 91–108.

Peng, D.-Y., Robinson, D.B., 1976. A New Two-Constant Equation of State. Ind. Eng. Chem. Fundam. 15, 59–64.

Rahbar, K., Mahmoud, S., Al-Dadah, R.K., Moazami, N., Mirhadizadeh, S.A., 2017. Review of organic Rankine cycle for small-scale applications. Energy Convers. Manag. 134, 135–155.

Tanaka, K., Ishikawa, J., Kontomaris, K.K., 2017. Thermodynamic properties of HFO-1336mzz(E) (trans-1,1,1,4,4,4-hexafluoro-2-butene) at saturation conditions. Int. J. Refrig. 82, 283–287.

Valtz, A., Coquelet, C., Richon, D., 2004. Vapor–liquid equilibrium data for the sulfur dioxide (SO2) + 1,1,1,2,3,3,3-heptafluoropropane (R227ea) system at temperatures from 288.07 to 403.19 K and pressures up to 5.38 MPa: Representation of the critical point and azeotrope temperature dependence. Fluid Phase Equilibria 220, 75–82.

List of figures

List of tables